Fracture Processes in Concrete and Fiber Reinforced Cementitious Composites

By Victor C. Li,[1] M. ASCE and Erwin Liang[2]

Abstract: This paper discusses the fracture processes of concrete and fiber reinforced cementitious composites with special focus on the development of the fracture process zone with respect to the stress-separation constitutive relation of such materials. The suggestion is that the overall mechanical behavior of a concrete or FRC structure could be strongly influenced by the stress-separation constitutive relation, which in turn could be altered by engineering the microstructure of the material, especially in FRC. The process zone length is found not to be a material property, but depends on the geometry of the specimen and the loading configurations. All these results are shown explicitly by a simple numerical model of a center-cracked panel subject to remote edge loading or to wedge loading on the crack faces. These calculations also provide further understanding to the validity of certain failure criteria.

Introduction

In concrete, microcracks in the cement may form as a result of drying shrinkage. Often, the interface between the aggregates and the cement matrix forms a weak bond. Using X-ray techniques, Slate (24) found that bond cracks occur at applied stresses of the order of 30% of the compressive failure stress level in his concrete specimens while matrix cracks occur at a slightly higher stress level. Diamond and Bentur (6) showed that the joining of these cracks to form major throughgoing ones takes a tortuous path, since the cracks often propagate by winding around the aggregates. Using a scanning electron microscope under carefully controlled compact tension tests, they found that crack "ends" tend to be branched, often run through cement matrix material and sand grains, and are often discontinuous. An interpretation of the winding cracks on the microscopic level is that the failure process of concrete involves the pulling out of the aggregates from the cement matrix, as the aggregates generally have a higher strength than either the cement matrix or the interfacial bond. Presumably, the increased apparent fracture toughness of concrete over cement paste (see, e.g., Ref. 25) comes from this aggregate "pull-out" or bridging effect. In short strand FRC, the bridging effect is dominated by the fibers. It is the work to cause fiber pull-out or breakage that contributes to the significant increase in the ductility of FRC.

The constitutive relation between increasing (localized) material separation w and the traction σ_c carried across the cracking material (e.g., in a uniaxial test) will be called the stress-separation curve (or the σ_c-w curve). The basic assumption for the existence of the stress-separation curve is that the diffuse damage in a given material localizes onto a narrow zone (or a plane on the continuum scale) due to stress concentration associated with material inhomogeneity or structural geometry (such as a notch). The use of a stress-separation relationship rather than a stress-strain relationship in describing the inelastic deformation in the process zone is related to the brittle behavior of the cement matrix, which results in microcracking, and to the bridging effects across a crack plane by aggregates and/or fibers as mentioned above. This is in contrast to the plastic deformation in a volume of material for ductile metals, which is better described by a stress-strain relationship. Based on the above brief description of the physical processes of fracture in concrete and in FRC, it should be clear that the stress-separation curve must reflect the energy dissipation connected with pull-out of aggregates and/or fibers, microcrack branching, tip blunting by voids, and all other possible energy absorption mechanisms. In fact, the area under the stress-separation curve provides a measure of the fracture toughness or the critical energy release rate (see, e.g., Ref. 22 and Eq. 5). In addition, these mechanisms should control the shape of the stress-separation curve. For example, in concrete the average aggregate size and aspect ratio, and the bond strength between aggregate and cement (which depends on the surface roughness of the aggregates and chemical bonding) should have dominant effects on the stress-separation curve shape. Similar considerations apply to the fibers in FRC. It may be expected that fiber types, lengths, cross-sectional geometry, surface treatment, volume fractions, etc., all contribute to affect the stress-separation curve. In general, the bridging action of the fibers in FRC provides a long tail in the stress-separation curve. These observations suggest that it is possible to engineer the fiber mechanical and geometrical properties to obtain desirable macroscopic behavior in FRC through the stress-separation curve. This begs the question: How does the stress-separation curve shape influence the behavior of a concrete or FRC structural component when cracks are involved?

In this paper, we attempt to study the development of the inelastic fracture process zone with respect to load level, loading configuration, structural geometry and most importantly, the constitutive or the stress-separation relation in the process zone. In turn, the development of the process zone controls the behavior of the structural component. It also provides some insight into the adequacy/inadequacy of certain proposed toughness characterization in FRC and in concrete. This study is based on a numerical analysis of a simple structure—a center-cracked panel, which is assumed to behave elastically everywhere except inside the process zone, which follows a prescribed stress-separation relationship. The simple center-cracked panel geometry is chosen because of the simplicity it allows in the formulation of the numerical analysis. Also, in the limiting situations where strength criteria or linear elastic fracture mechanics applies, some analytic solutions are known in very simple forms. In addition, with slight modifications, certain laboratory experiments could be simulated. Correspondence between experimental results and our numerical solutions provides confidence in our analytic and numerical procedures.

[1]Assoc. Prof., Dept. of Civ. Engrg., Massachusetts Inst. of Tech., Cambridge, MA 02139.

[2]Grad. Research Asst., Dept. of Civ. Engrg., Massachusetts Inst. of Tech., Cambridge, MA 02139.

Note.—Discussion open until November 1, 1986. To extend the closing date one month, a written request must be filed with the ASCE Manager of Journals. The manuscript for this paper was submitted for review and possible publication on May 21, 1985. This paper is part of the *Journal of Engineering Mechanics*, Vol. 112, No. 6, June, 1986. ©ASCE, ISSN 0733-9399/86/0006-0566/$01.00. Paper No. 20666.

The paper is organized in the following manner: A description of the problem formulation is first given. Then the material models of the stress-separation behavior are presented. This is followed by a description of the development of the fracture process zone and their control by the σ_c-w curve shape, the loading configuration and by the structural geometry. These considerations provide the necessary background for discussions of some implications on fracture characterization of concrete and FRC.

Problem Formulation

Referring to Fig. 1 of a center-cracked panel loaded by a uniform tensile stress σ_o as shown, and assuming now that the panel width $W \to \infty$, stress equilibrium (in the y direction) on the crack line requires that the stress (yy component) on the crack line

$$\sigma(x) = \sigma_o - \int_c G(x - x') \frac{\partial w(x')}{\partial x'} dx' \quad \ldots\ldots (1)$$

where c denotes the line of (opening) displacement discontinuity $w(x)$ and may be recognized as the total crack length. The Green's function $G(x - x')$ gives the stress at a point x due to a unit dislocation located

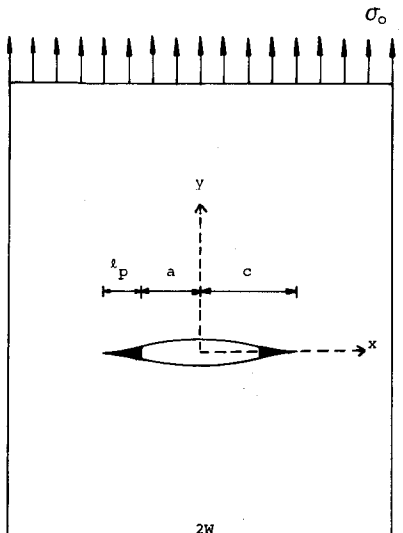

FIG. 1.—Geometry of Center-Cracked Panel Numerically Modeled in Present Study; Traction Free Crack (TFC) with Length a and Process Zone with Length l_p Make Up Total Crack of Length c

at a point x'. The term $-[\partial w(x')/\partial x']dx'$ represents the distribution of dislocations along c, and is treated as an unknown to be solved as part of the solution. A simple interpretation of Eq. 1 is that the stress would be equal to σ_o at any point x in a homogeneous plate with no cracks. In the presence of a crack, the stress is perturbed by the amount represented in the integral term. The representation of crack openings with a continuous distribution of edge dislocations follows the work of Bilby and Eshelby (5) and Rice (22). For a linear elastic body in plane strain, the Green's function is (see, e.g., Ref. 12):

$$G(x - x') = \frac{E}{4\pi(1 - \nu^2)} \frac{1}{x - x'} \quad \ldots\ldots (2)$$

where E = the elastic Young's Modulus; and ν = the Poisson Ratio. To complete the problem formulation, appropriate boundary conditions must be prescribed on the crack of length $2c$. On the traction-free part (hereafter called the traction-free crack or TFC with length a), the stress is simply zero. In the process zone l_p where traction transfer exists, neither the stress nor the opening displacement is known a priori. However, we assume that material deformation in this zone obeys a certain stress-separation behavior, a σ_c-w relationship obtained from experiments. Available σ_c-w relationships can be found in (9,10,20,21,27,29) for concrete and mortar and for some FRC. To illustrate, Fig. 2(a) shows several experimental σ_c-w curves for steel FRC (after Wecharatana and Shah, Ref. 29) and Fig. 2(b) shows some typical σ_c-w curves for concrete and FRC (after Hillerborg, Ref. 11). Thus

$$\sigma_c = \sigma_c(w) \quad \ldots\ldots (3)$$

for a given material.

The total crack length c responds to the stress field (surrounding the tip of the total crack), which in turn depends on the applied load and the geometry of the structure. Hence, a certain cracking criterion is necessary to determine the proper value of l_p and c (or any pairings of a, l_p and c) for a given applied load. Following Dugdale (7) and Barenblatt (1), we assume that the process zone will have a size appropriate to the surrounding elastic stress field in a way such that the stress will transit smoothly from outside to inside the process zone. This implies that the stress singularity assumed in linear elastic fracture mechanics will be absorbed into the inelastic deformation (the process of decreasing traction with increasing opening) in the process zone. Furthermore, the material ahead of the total crack becomes part of the process zone as soon as the (ultimate) tensile strength f_t is reached. Inside the process zone, the stress decays from f_t to zero at the tip of the traction free crack, the rate of decay being consistent with the stress-separation behavior. It can be shown (see Ref. 17 for detail) that this assumed fracture criterion is also consistent with smooth closing at the tip of the total crack, i.e., $dw/dx|_{x=c} = 0$. The fracture criterion is implemented by ensuring that at $x = c$ the stress intensity factor K_s due to the closing traction in the process zone cancels the stress intensity factor K_o induced by the applied load. Hence

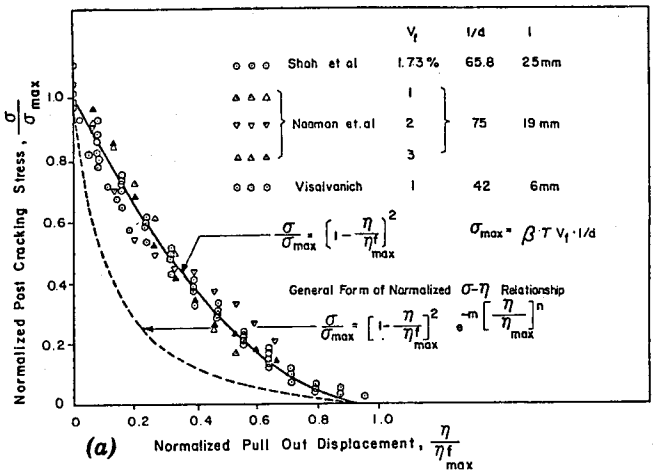

FIG. 2.—Stress-Separation Relations: (*a*) For Steel FRC (after Wecharatana and Shah Ref. 29); and (*b*) for Plain and Fiber-Reinforced Mortar and Concrete (after Hillerborg Ref. 11)

$$K_o + K_s = \sigma_o\sqrt{\pi c} - 2\sqrt{\frac{c}{\pi}}\int_a^c \frac{\sigma_c(x)}{\sqrt{c^2 - x^2}}\,dx = 0 \quad \ldots\ldots\ldots\ldots\ldots\ldots \quad (4)$$

Rice (22) pointed out that the cohesive zone model described above is exactly equivalent to the Griffith crack model in the case when the process zone size l_p is small compared to all other characteristic dimensions in the structure. Eqs. 1 and 3 form a nonlinear singular integral equation in $w(x)$ and are supplemented by Eq. 4. A Gauss-Chebyshev integration formulation (see, e.g., Ref. 8) is used for discretization and integration, and the Newton-Raphson iteration scheme is used to solve the resulting set of nonlinear algebraic equations. Full details of the numerical methodology can be found in Ref. 17. In what follows, after introducing the stress-separation constitutive models adopted for this study, we discuss some results and interpretations of several analyses based on the formulation just described.

Stress-Separation Constitutive Models

Two stress-separation constitutive models, shown in Figs. 3(*a–b*), are used in the analyses. Focus is placed on the effects of the shape of the stress-separation curves on the development of the process zone, and on the overall structural behavior of the center-cracked panel. Model 1 is a linear straight line descending from the tensile strength f_t at zero material separation to zero stress at the critical separation w_c. This linear decay model has been used by Hillerborg (11). Model 2 has a rapid drop

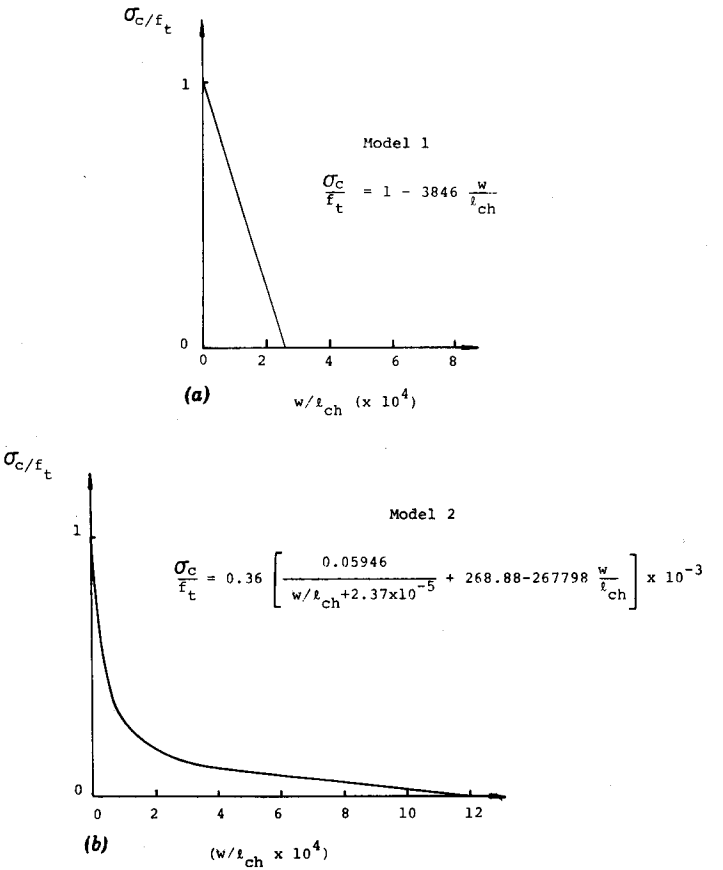

FIG. 3.—Stress-Separation Constitutive Models Used for Numerical Analysis in this Study; Both Models Have Same G_c and f_t but Shapes Are Quite Different with Very Small Critical Separation Distance w_c for: (*a*) Model 1, and Much Larger w_c for (*b*) Model 2

in traction transfer σ_c with separation w, followed by a long tail (large w_c). This model has been used by Ingraffea and Gerstle (13). In general, FRC has large w_c values since w_c in FRC may be taken as half the fiber lengths (29). Of course, the appropriate model to use in a given analysis is the one which best describes the material under consideration. In this paper, we treat them as two contrasting cases, in the sense that for a given tensile strength f_t and a given critical energy release rate G_c, Model 1 has a much smaller critical material separation w_c when compared to Model 2. We note in passing that G_c is given by the area under the stress-separation curve (22), i.e.,

$$G_c = \int_0^{w_c} \sigma_c(w)dw \quad \ldots\ldots (5)$$

As material properties, we have chosen $f_t = 2.0$ N/mm^2, $G_c = 0.039$ N/mm, $E = 21{,}500$ N/mm^2, and $\nu = 0.18$ as typical values for concrete. This choice of f_t and G_c gives $w_c = 0.028$ mm for Model 1 and $w_c = 0.127$ mm (approximated in calculations) for Model 2. The range of w_c falls into the range of observed values for concrete in direct tension tests (10,20,21) and in compact tension tests (16), although the w_c value is often poorly determined in direct tension tests (e.g., Ref. 10). We define a material characteristic length $l_{ch} = EG_c/f_t^2$. For the above values of E, G_c and f_t for concrete, $l_{ch} = 107$ mm. Typical values of l_{ch} for glass fiber reinforced mortar is 0.5–3 m and for steel fiber reinforced concrete is 2–20 m (11). Hillerborg (11) suggested the use of l_{ch} to normalize all dimensions of structures. We have used it to normalize all length dimensions including the separation distance w. [This corrects an error in a previous paper by the first writer (16) who attributed the normalization of w by l_{ch} to Hillerborg (11).] While l_{ch} has no direct physical interpretation, Rice (23) showed that the process zone length is approximately proportional to l_{ch}. All stress quantities are normalized with respect to f_t in presenting results of numerical analyses.

Development of Fracture Process Zone

We study the development of the process zone with respect to three different controlling factors: the stress-separation constitutive behavior, the loading configuration, and the geometrical size. Where appropriate, comparisons to published experimental or numerical results are made. Implications to some proposed characterization of fracture toughness in concrete and FRC are suggested in the following section. The discussion in this section refers to Figs. 4–9. Three cases are analyzed, the remote uniformly loaded panels with Model 1 and Model 2 are labeled RU1 and RU2 in these figures, and the center wedge loaded panel with Model 2 has been labeled CL2.

Control of Process Zone Development by σ_c-w Curve.—Fig. 4(*a*) shows the calculated overall load-deformation behavior of the center-cracked panel shown in Fig. 3. Deformation is measured as crack opening displacement (COD/2) at $x = 0$. The analysis assumes an initial (half) notch length $a_o = 127$ mm $= 1.2l_{ch}$ and $W = \infty$. The two curves are for the two different constitutive models described in Fig. 3. Clearly Model 1 allows the structure to reach a higher peak load (at $0.47f_t$), about one and a half times that of Model 2 (at $0.3f_t$). At the same time the descending branch is much sharper in the load-deformation curve for Model 1 than that for Model 2. These behaviors make the structure seemingly stronger (with higher tensile strength) but more brittle for Model 1. This result is particularly interesting in view of the fact that the only difference in these models lies in the shape of the stress-separation curve, while all material parameters, including the critical energy release rate G_c remain the same.

As a check on our calculations, the parameters used in Model 2 has been chosen to correspond to those of Ingraffea and Gerstle (13) who

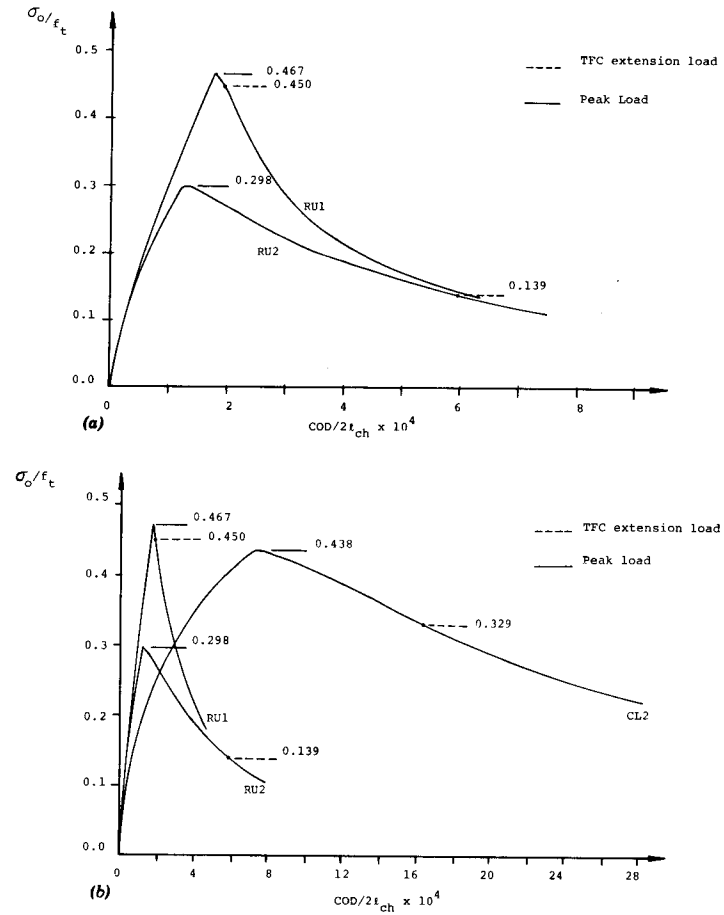

FIG. 4.—(*a*) Normalized Load Applied at Remote Edges of the Center Cracked Panel versus Normalized Opening Displacement at Crack Center, for Model 1 (RU1) and for Model 2 (RU2). Distinctive Behavior between RU1 and RU2 Is Mainly Contributed by Difference in w_c Values between Model 1 and Model 2; (*b*) Same as Part *a*, with New Curve for Model 2 but with a Wedge Load Applied to Crack Faces (CL2); Demonstrates Influence on Development of Process Zone by Loading Configuration

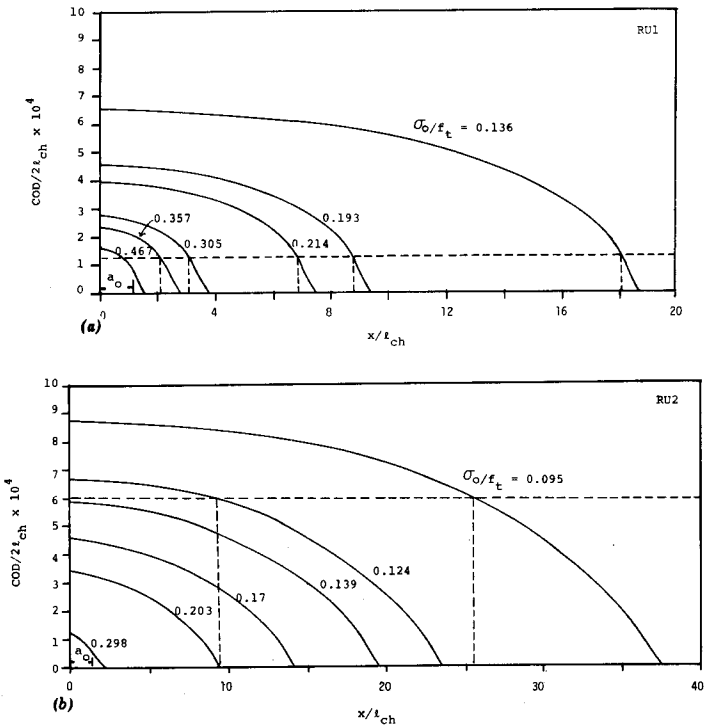

FIG. 5.—Crack Face Profiles (Only One-Quarter Shown Due to Symmetry with Respect to Both Axis). Horizontal Dotted Line is Value of w_c. Its Intersection with Crack Profiles Indicates Tip of Traction Free Crack: (*a*) For RU1 at Different Values of Remote Load σ_o; and (*b*) for RU2

did a similar analysis (based on their model D) using the finite element method as the numerical tool. We found that the COD at $x = 0$ at peak load are within 1% of each calculation, while the peak load itself has some discrepancies amounting to about 15% (lower in our calculated result). Although Ingraffea and Gerstle used a panel width less than four times the longest total crack length in their analysis to approximate a panel of infinite width (and height), the error (if any) should have lowered his calculated peak load, as we shall explain in a later section of this paper. Other possibilities influencing the calculation accuracy are the fineness of his mesh or our discretization, and the stiffness of the elements near the crack line in the mesh. The discrepancy may also be related to the use of quarter-point singular elements at the initial notch tip in Ref. 13, which may have an important influence on the maximum load achievable. This discrepancy does not affect our conclusion regarding the influence of the shape of the σ_c-w curve on the structural behavior.

To appreciate the cause of the σ_c-w shape influence on the structural behavior, it is necessary to investigate the growth of the process zone

in response to applied loads for the two models. Following Ref. 13, we show the (half) crack opening displacement at various load stages in Figs. 5(*a–b*). In these figures, the horizontal dash line indicates the critical material separation w_c. Thus the intersections of this line and the crack opening profiles are the locations of the tip of the traction free crack (TFC). For each Model, there is relatively little growth of the process zone prior to peak load, as shown by the shortest crack profile in

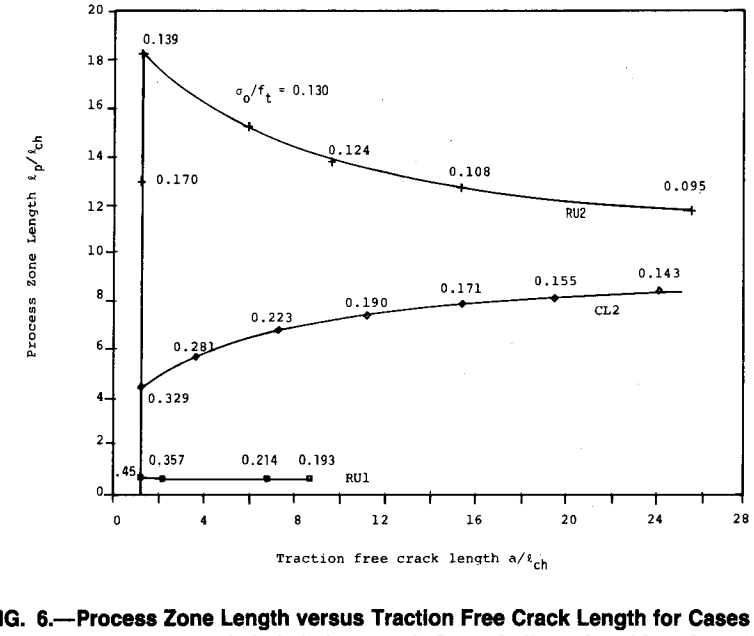

FIG. 6.—Process Zone Length versus Traction Free Crack Length for Cases RU1, RU2 and CL2. Numbers Labeled along each Curve Indicate Load Level (σ_o/f_t) Associated with Particular Values of l_p and a

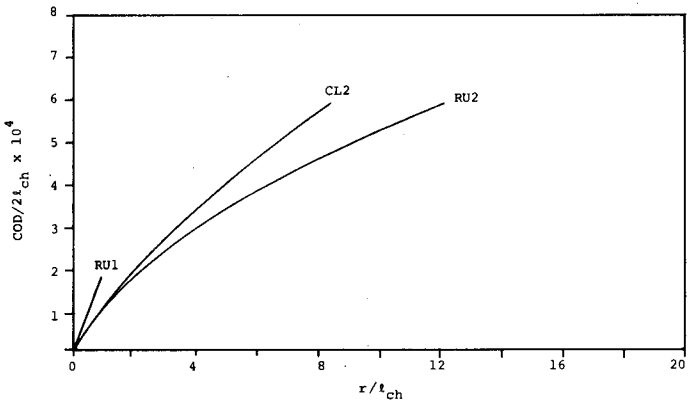

FIG. 7.—Different Shapes and Sizes of Crack Face Opening Profiles in Process Zone for RU1, RU2, and CL2, All at Steady-State Condition

Figs. 5(*a–b*). The expanding crack profiles correspond to decreasing equilibrium load levels on the descending branch of the load-deformation curve [Fig. 4(*a*)]. For Model 1 just below peak load (at 0.45 f_t), extension of the TFC occurs, with very little further change in the length of the process zone size, i.e., the crack tip region simply translates to the right, as can be seen in Fig. 5(*a*). In contrast, the extension of the total crack in Model 2 occurs with an extension of the process zone, while the TFC length does not change until the load decreases to 0.14 f_t. The last crack profile before TFC extension is shown by the curve labeled (σ_o/f_t =) 0.124 in Fig. 5(*b*) for Model 2. The peak loads and the TFC extension loads for the two models are indicated in Fig. 4(*a*). Thus high strength is prohibited for Model 2 because of the early extensive growth of the process zone, which is somewhat analogous to the large scale plastic deformation in a ductile metal sheet.

Fig. 6 summarizes the growth of the process zone as a function of the TFC length. Again, for Model 1 (symbols □), a small steady state process zone length ($0.7l_{ch}$) is reached with very little TFC growth. For Model 2 (symbols +), the process zone size in fact over-extends itself before decreasing to a high steady-state value ($11.2l_{ch}$) accompanied by TFC growth. This same phenomenon for Model 2 is also found by Ingraffea and Gerstle (13). For further illustration, we show in Fig. 7 the opening displacements in the process zone at steady state. Model 1 (RU1) has a much smaller but sharper opening process zone while Model 2 (RU2) has a much larger but more gradual opening process zone. The observation just presented suggests that the process zone size is strongly influenced by the material model (the stress-separation behavior) in the process zone. However, it should be pointed out that the process zone growth also responds to the loading configurations (to be discussed next).

The steady-state process zone size $(l_p)_{ss}$ may be estimated by assuming $K_0 = K_{Ic} = \sqrt{G_c E}$ in Eq. 4 and assuming that $\sigma_c(x)$ vary linearly from f_t to 0 in the process zone. This procedure was first used by Palmer and Rice (19) who studied the "slip-weakening" process in consolidated clay slopes under shear deformation. Thus

$$(l_p)_{ss} = \frac{9\pi}{32}\left(\frac{E}{1-\nu^2}\right)\left(\frac{G_c}{f_t^2}\right) \quad \ldots\ldots (6)$$

Evaluation of Eq. 6 gives $(l_p)_{ss}/l_{ch}$ = 0.9. This is remarkably accurate for Model 1 but misses by an order of magnitude when applied to Model 2. Clearly the problem lies in the assumption of a linear variation of σ_c in the process zone. This assumption is adequate for a material with a linear stress-separation curve but is inadequate for a material with a stress-separation curve as shown in Fig. 3(*b*).

Control of Process Zone Growth by Loading Configuration.—To investigate the influence of loading configuration on the development of the process zone, we use the same center-cracked panel structure shown in Fig. 1, but with loading applied locally at the center of the crack line $x = 0$ (Case CL2). This is equivalent to a point wedge load forcing the crack face to open. The resulting load-deformation relationship is shown in (symbols ◇) Fig. 4(*b*), which also includes that for Model 1 and 2 for remote loading for comparison purposes. The σ_o values for CL2 are defined as the wedge load divided by the total crack length 2*c*. The figure shows that, with all material parameter and structural geometry the same (as for RU2), the center loaded panel structure reaches a peak load at a much larger COD and a more gradual descending branch. Traction free crack growth occurs at 0.33 f_t, when the process zone length is still extending (Fig. 6, symbols ◇). The steady-state process zone length ($8.1l_{ch}$) is lower than that for the remotely loaded configuration. This can also be seen in Fig. 7 (compare CL2 profile to RU2 profile). Clearly the process zone development is responding to the stress fields that drives the process zone and the TFC extension. The wedge load causes the crack face to open up while a compressive stress may be induced by

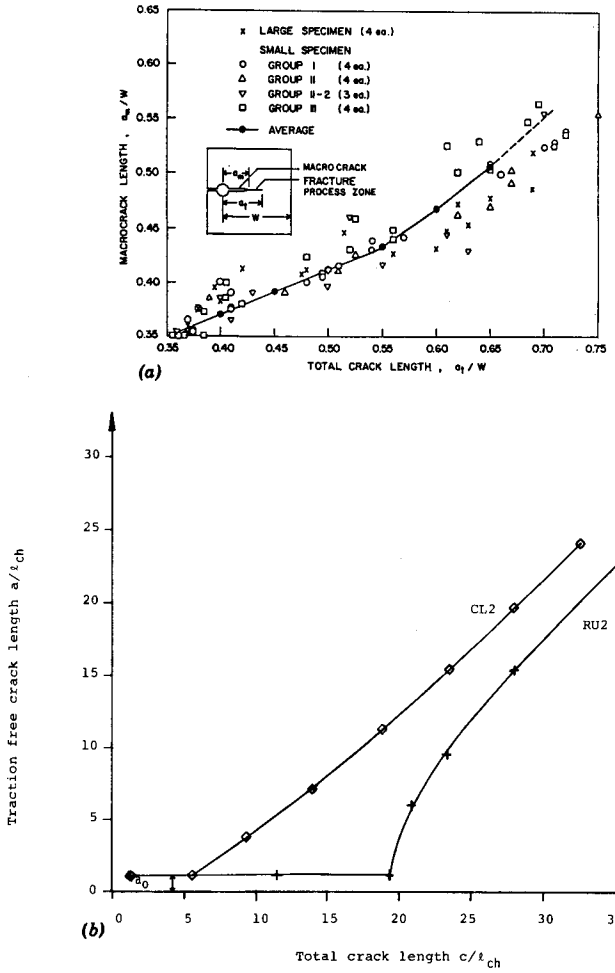

FIG. 8.—Traction Free Crack Length versus Total Crack Length Obtained: (*a*) From Wedge-Loaded Edge Crack Specimens by Kobayashi et al. (14); and (*b*) from Present Numerical Analysis

bending ahead of the process zone which keeps it from extending. This combined action results in a smaller process zone length than that for remote loading, and a monotonically increasing process zone size as shown in Fig. 6. This comparison illustrates the fact that in general the development of the process zone and its steady-state size in concrete or FRC is not a material property, but rather depends on the loading configuration (and on the structural geometry).

The center-cracked panel loaded at the center as just described should qualitatively simulate the loading of a compact tension specimen. Majumdar and Walton (18) reported that in compact tension tests of asbestos cement by Lenain and Bunsell (15), three distinct stages of crack growth were observed: "(1) Creation of a zone of microcracks in front of the visible crack, (2) growth of this zone together with slow stable crack growth and (3) extension of the principle crack while the size of the microcrack zone remains constant." This is exactly what Fig. 6 (symbol ◇) suggests.

In another experimental program, Kobayashi et al. (14) carried out some wedge loaded compact tension tests on concrete specimens. Employing a replica technique, they claimed to be able to measure the growing crack lengths accurately. Fig. 8(*a*) shows some of their experimental results. For comparison, Fig. 8(*b*) shows the data replotted from Fig. 6 in the form of traction free crack length versus total crack length. The increasing slope with total crack length for the presently simulated center loaded panel solution [symbol ◇ in Fig. 8(*b*)] qualitatively reproduces that of the experimental data by Kobayashi et al. while the curve for the remote uniformly loaded case [symbol + in Fig. 8(*b*)] appears to be quite different. Given the above discussions of the control of the process zone development by the surrounding stress field, this correspondence should be expected. However, no attempt is made for a detail comparison, since the constitutive tension softening relation for the material used in the above mentioned experimental test is not known to us. Also our numerical simulation is for a panel of infinite width, while the compact tension specimens have finite widths.

Control of Process Zone by Structural Geometry.—A simple way of introducing geometric effects is by considering a center-cracked panel with finite width W. In this case, the Green's function in Eq. 1 is given by (see, e.g., Ref. 4)

$$G(x - x') = \frac{E}{4W(1 - \nu)} \frac{\cos\left(\frac{\pi x'}{W}\right)}{\sin\left(\frac{\pi x}{W}\right) - \sin\left(\frac{\pi x'}{W}\right)} \quad \ldots\ldots\ldots\ldots\ldots\ldots (7)$$

and the calculation proceeds as before. This formulation is based on the symmetry of an extended panel with periodic collinear cracks. The induced normal stresses acting on the side-walls (amounting to a few percent error) are ignored. Further details are contained in Liang (17).

Fig. 9 shows the load-deformation curve for three different ratios of initial crack length to panel width (a_o/W) using Model 1. The top-most curve ($a_o/W = 0$) retraces that in Fig. 4(*a*) where the panel width has

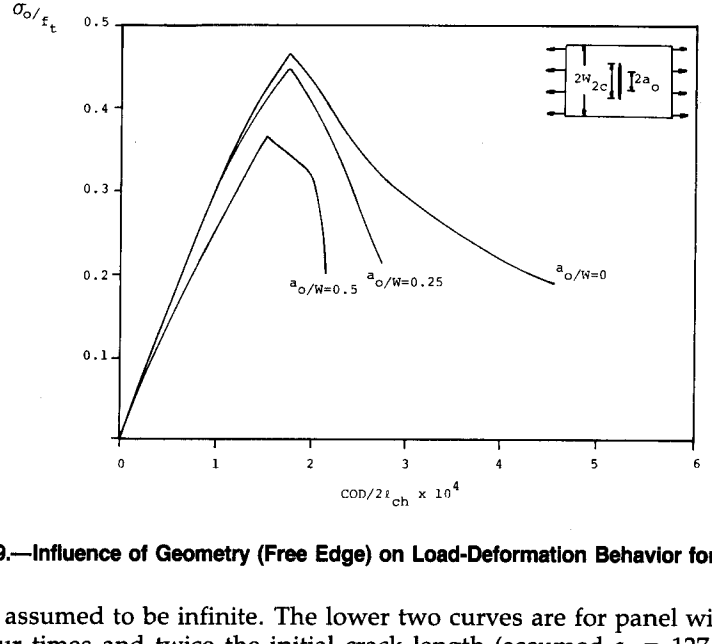

FIG. 9.—Influence of Geometry (Free Edge) on Load-Deformation Behavior for RU1

been assumed to be infinite. The lower two curves are for panel widths of four times and twice the initial crack length (assumed a_o = 127 mm or $1.2l_{ch}$). Clearly as the free edge of the plate is sensed by the approaching crack, the structure behaves more compliantly and also decreases in load carrying capacity. The shape of the unloading branch for $a_o/W = 0.5$ also suggests the possibility of an unstable "pop-through." Again, these structural behaviors are related to the development of the process zones, which in turn are influenced by the structural geometry, in this case, the presence of a free edge.

Implications on Fracture Characterization

The preceding discussions on the development of the process zone and the associated influence on structural behavior provides some insight on the appropriateness of some proposed characterizations of fracture resistance in concrete and in FRC. The present analysis explicitly accounts for the presence of a process zone undergoing inelastic deformation described by a stress-separation curve and therefore constitutes a nonlinear fracture analysis. In special limiting cases, the resulting predictions based on such an analysis should correspond to that based on linear elastic fracture mechanics, or that based on strength concepts. Where the special limiting conditions are not met, the nonlinear analysis must be used to provide an accurate description of the fracture process. This corresponds to what Bažant (2) called the size effect law.

It is interesting to consider the tensile load carrying capacity of a structural member (or that of a laboratory specimen). In the ideal case where no crack exists in the structure, the maximum stress corresponding to the peak load should be exactly equal to the tensile strength f_t. In the case where a large crack exists (large here is in reference to process zone

size), LEFM applies since the small scale yielding condition is satisfied. This means that the crack tip is dominated by a K-field (i.e., a stress field whose intensity is characterized by a stress intensity factor K_I), and the load carrying capacity is determined by the crack size and the fracture toughness (K_{Ic}) of the material, which results in a maximum applied stress smaller than f_t. This is often termed "brittle fracture." Between these two limiting conditions, the process zone is of comparable size with the traction free crack length and its presence must be explicitly accounted for. Fig. 11 summarizes these situations for the center-cracked panel structure (with $W = \infty$). In this figure, the normalized maximum applied stress (σ_p/f_t) achievable corresponding to the peak load is plotted against a normalized initial notch length measure ($\sqrt{l_{ch}/\pi \cdot a_o}$). Prediction of peak load based on strength criteria is shown as the horizontal dash line. Prediction based on LEFM is shown as the other dash line with a slope of unity. The calculated peak load based on the present nonlinear analysis is shown as the solid lines for each of the two stress-separation models. The aforementioned limiting situations can be seen on the lower left corner and the upper right-hand corner of the plot. The use of a_o as a measure of crack size is justified by the fact that very little real (traction-free) crack extension occurs prior to peak load (see, e.g., Fig. 6) and hence a_o may be regarded as approximately the actual traction-free crack length at peak load.

Comparing between the two models, Model 1 appears to allow a larger range of validity for LEFM and also seem to approach the strength criteria easier (at larger value of a_o) in comparison to Model 2. The reason, of course, lies in the fact that Model 2 produces a larger process zone due to its larger value of w_c. This suggests that for material of the type Model 2 represents, it is more likely that a nonlinear analysis is required, everything being the same. Since G_c has the same value for both models, and hence the same value for l_{ch}, this analysis reveals w_c as an independent parameter controlling the validity of LEFM applications. For example, it has been proposed that for LEFM to be valid (see, e.g., Ref. 11), the beam depth d in a 3-point bend test should satisfy the criterion $d > 10\text{–}15 l_{ch}$ for concrete. Fig. 10 suggests that for concrete and FRC, LEFM validity requires $d > \alpha(w_c)\, l_{ch}$, where α is an increasing function of w_c. The exact dependence of α on w_c can be obtained from a nonlinear analysis as carried out in this paper. Although it might be expected that qualitatively, the plot of Fig. 10 is rather universal, the exact details of the solid curves must depend on the particular geometry of the structure or specimen, as well as on the loading configuration, due to the dependence of the process zone development on these parameters as explained in the previous paragraphs.

It appears to be a popular notion that the peak load corresponds to a certain critical state associated with "crack propagation." This is apparently true for ideally brittle material where LEFM applies because the peak load in this case corresponds to a critical stress intensity factor equal to the fracture toughness. Even when LEFM is recognized not to be valid, the peak load has still been associated with a certain critical state and a critical effective crack length which accounts for the presence of the process zone (28). We shall examine whether this is a sensible approach.

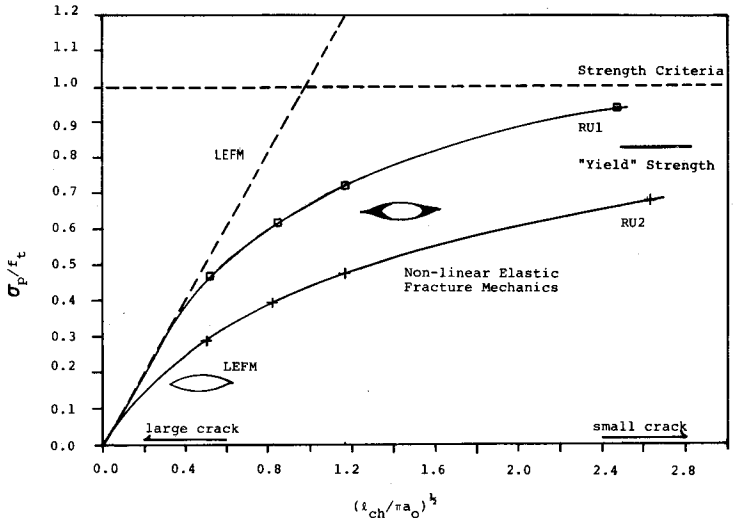

FIG. 10.—Size Effect on Achievable Peak Load; Present Nonlinear Analysis Approaches Predicted Peak Loads by LEFM and Strength Criteria under Limiting Conditions

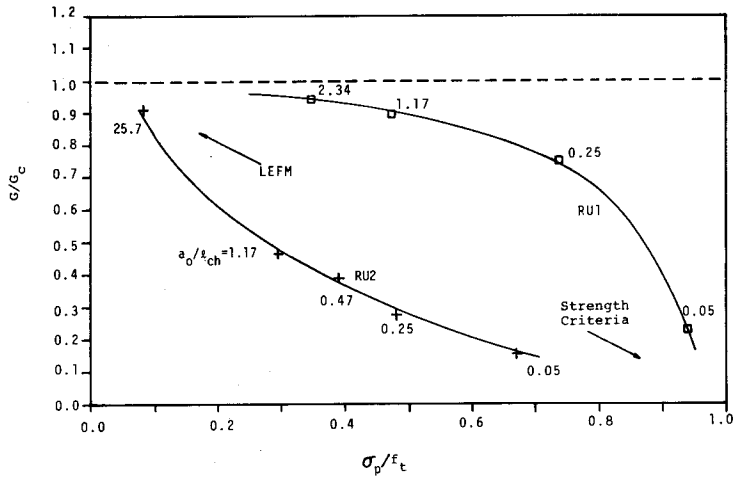

FIG. 11.—Energy Release Rate at Peak Load for Various Crack Sizes; Upper Left Corner Represents the Case Where $G \rightarrow G_c$ at Peak Load as Predicted by LEFM. Otherwise, Direct Application of LEFM Using Peak Load May Be Expected to Underestimate G_c or K_{Ic}

For a given initial notch length a_o, it is possible to calculate a corresponding peak load, as shown in Fig. 10. It is also possible, at peak load, to calculate the energy release rate G by computing the J-integral using a contour surrounding the process zone, since (e.g., Ref. 22):

$$G = J = -\int_a^c \sigma_c(x) \frac{\partial w(x)}{\partial x} dx \quad \ldots\ldots (8)$$

The result of G (normalized by G_c) is plotted as a function of the peak load in Fig. 11, again for the two material models. For small a_o (lower right corner of figure), the peak load again reaches the tensile strength indicating the validity of the strength criteria, and the energy release rate G is only a small fraction of G_c at peak load. For large a_o (upper left-hand corner of figure), the peak load is only a small fraction of the tensile strength but the energy release rate reaches G_c, indicating the validity of LEFM. In between these two limits, however, and especially for Model 2, the energy release rate at peak load can be substantially below G_c. Thus, the process zone continues to grow after peak load without extension of the real (traction free) crack for Model 2, as was indicated in Figs. 4(*a*) and 6. To understand this phenomenon, consider a given a_o. At peak load, the process zone length for Model 2 is much longer than for Model 1 (see Fig. 6). This implies that the stress at the TFC tip for Model 1 is much more focused and therefore provide a higher traction free crack driving force, while the driving force for Model 2 at peak load may be much lower than G_c. In view of the preceding discussion, it may be erroneous to associate the peak load with a failure or fracture load for a material with stress-separation behavior representable by Model 2.

Is it meaningful to compute the fracture toughness by applying LEFM based on the peak load and an effective (traction-free) crack length? Presumably an effective crack length is used: (1) To correct for the presence of the process zone; and (2) to overcome the practical difficulty of locating the "crack tip" as explained in the introduction of this paper. A common procedure to obtain the effective crack length a_e is to measure experimentally the crack mouth opening displacement (e.g., the CMOD in a 3-point bend test specimen) at peak load σ_p. Then

$$a_e = f(\sigma_p, \text{CMOD}_p; E) \quad \ldots\ldots (9)$$

where the function f is based on an elastic analysis of the particular specimen geometry. For the center-cracked panel under uniform remote load (Fig. 1), this function is simply

$$a_e = \frac{E \cdot \text{CMOD}_p}{2(1-\nu^2)\sigma_p} \quad \ldots\ldots (10)$$

where CMOD_p = half the crack opening at the center. That is, CMOD_p = COD/2 shown in Fig. 4(*a*) at peak load. (Here, we have numerically simulated the experiment.) Applying LEFM, it is possible to calculate the stress intensity factor or the energy release rate at peak load, i.e.,

$$G_p = g(\sigma_p, a_e) \quad \ldots\ldots (11)$$

Again the function g depends on the particular specimen geometry and

could be found from fracture handbooks (such as Ref. 26). For the center-cracked panel

$$G_p = \frac{\pi \sigma_p \text{CMOD}_p}{2} \quad \ldots\ldots (12)$$

The idea is to associate G_p with the critical energy release rate G_c. The validity of such an association appears to depend on the details of the stress-separation curve. Referring to Fig. 4(*a*), and using numerical values quoted earlier (following discussion of Eq. 5), Model 1 has CMOD_p = 0.02 mm and σ_p = 1.308 N/mm^2, which gives a_e = 169 mm and G_p = 0.041 N/mm according to Eqs. 10 and 12. These results suggest that an effective extension of 37 mm of traction free crack length has occurred at peak load. The calculated value of G_p is within 5% error from the actual G_c value (0.039 N/mm). Note that a direct application of LEFM using the initial notch length a_o = 127 mm would have given G_p = 0.031 N/mm, which is more than 20% less than G_c. For Model 2, CMOD_p = 0.014 mm and σ_p = 0.834 N/mm^2, which gives a_e = 186.0 mm and G_p = 0.019 N/mm. Thus the critical energy release rate would be underestimated by more than 50%. According to the foregoing discussion, it would appear that the correction procedure applied to LEFM by means of an effective crack length is appropriate to material of Model 1 type and definitely not appropriate to material of Model 2 type for which w_c is large.

Summary and Conclusions

This paper analyzes the fracture processes of concrete and fiber reinforced cementitious composites by means of a simple numerical model which explicitly accounts for the inelastic deformation in the fracture process zone. The development of the process zone is studied with respect to the stress-separation constitutive behavior, the loading configuration and the structural geometry. The analysis provides a framework for understanding the transition of a strength-based failure criterion to a linear elastic brittle crack failure criterion (i.e., LEFM). In between these limiting situations a nonlinear analysis becomes a necessity to properly describe fracture resistance of such materials. The size scale of process zones is such that typical laboratory specimens fall short of the small scale yielding condition for LEFM validity. Analyses in this paper lead to the following conclusions:

1. The use of LEFM for crack analysis in concrete and FRC structures are generally invalid unless all relevant structural dimensions d are much larger than the steady-state process zone size. For a material representable by Model 2, $(l_p)_{ss} = 10 l_{ch}$ (Fig. 6). This implies $d >> 1$ m for a concrete with l_{ch} = 100 mm, and $d >>$ 20–200 m for a steel FRC with l_{ch} = 2–20 m (11). These inequalities are necessary for the small scale yielding conditions (*ssy*) in LEFM to be satisfied. If *ssy* is not satisfied, then the stress-separation curve must be used as a fundamental material property in predicting crack formation and extension. Also apart from G_c, the shape of the stress separation curve plays an important role in determining the behavior of the structure, as shown in Fig. 4(*a*).

2. Attempts to simplify the characterization of fracture resistance, particularly those that are based on the association of crack growth with the peak load may be laid on questionable foundations. Even if an effective crack length is used to account for the presence of the process zone, the analysis may suffer significant inaccuracy, especially for materials with large w_c, such as in FRC.
3. While the stress-separation curve should be regarded as an important fundamental material property, the process zone length l_p, even in a steady state, is not a material property. Rather, l_p depends on the loading configuration and the structural geometry.

The analyses in this paper demonstrate the importance of the shape (not only the G_c) of the stress-separation curve in controlling the overall structural behavior, when the process zone size is not negligible compared to structural dimensions. It may be possible to take advantage of this by designing the microstructure of the material to obtain desirable macroscopic mechanical properties through engineering the stress-separation curve. In FRC, this might be achieved by optimization of the fiber type, geometry and volume fractions. The commercial availability of large variety of fiber types and processing techniques increasingly improves the viability of such a procedure. However, much more research in the micromechanics modeling of the stress-separation curve will be needed. This appears to be an important research topic in advancing the fiber cementitious composite technology.

Much of the analysis results and conclusions stated here also apply to materials other than concrete or FRC. For example, the crazing phenomenon in some structural plastics and the bridging processes in some fiber epoxies would produce an inelastic process zone like that discussed in this paper. There is a need to characterize the fracture resistance of such materials through the experimental determination of their stress-separation curves.

Acknowledgments

The writers acknowledge useful discussions with D. M. Parks and S. Barker. A. Hillerborg, H. W. Reinhardt and an anonymous reviewer provided comments that led to several improvements in the revised manuscript. This study was supported by partial funding from the MIT Sloan Foundation and the National Science Foundation.

Appendix.—References

1. Barenblatt, G. I., "The Mathematical Theory of Equilibrium Cracks in Brittle Fracture," *Advances in Applied Mechanics*, Vol. 7, Academic Press Inc., London, England, 1962, pp. 55–125.
2. Bažant, Z. P., "Size Effect in Blunt Fracture: Concrete, Rock, Metal," *Journal of Engineering Mechanics*, ASCE, Vol. 110, No. 4, 1984, pp. 518–535.
3. Bažant, Z. P., and Oh, B. H., "Rock Fracture via Strain Softening Finite Elements," *Journal of Engineering Mechanics*, ASCE, Vol. 110, No. 7, July, 1984, pp. 1015–1035.

4. Bilby, B. A., Cottrell, A. H., and Smith, E., "Plastic Yielding from Sharp Notches," *Proceedings Royal Society of London*, A.279, London, England, 1964, pp. 1–9.
5. Bilby, B. A., and Eshelby, J. D., "Dislocations and the Theory of Fracture," *Fracture*, Ch. 2, Vol. 1, H. Liebowitz, Ed., Academic Press, New York, N.Y., 1968, pp. 99–182.
6. Diamond, S., and Bentur, A., "On the Cracking in Concrete and Fibre-Reinforced Cements," *Applications of Fracture Mechanics to Cementitious Composites*, S. P. Shah, Ed., Martinis Nijhoff, pub., 1985, pp. 87–140.
7. Dugdale, D. S., "Yielding of Steel Plates Containing Slits," *Journal of Mechanics and Physics*, Vol. 8, 1960, pp. 100–108.
8. Erdogan, F., and Gupta, G. D., "On the Numerical Solution of Singular Integral Equation," *Quarterly of Mathematics*, 1972, pp. 525–534.
9. Evans, R. H., and Marathe, M. S., "Microcracking and Stress-Strain Curves for Concrete in Tension," *Materiaux et. Construction*, Vol. 1, No. 1, 1968, pp. 61–64.
10. Gopalaratnam, V. S., and Shah, S. P., "Post-Cracking Characteristics of Concrete in Uniaxial Tension," *Engineering Mechanics in Civil Engineering*, Vol. 2, A. P. Boresi, and K. P. Chong, Eds., 1984, pp. 1393–1398.
11. Hillerborg, A., "Analysis of One Single Crack," *Fracture Mechanics of Concrete*, F. H. Whittman, Ed., Elsevier Science Publishers, The Netherlands, 1983, pp. 223–249.
12. Hirth, J. P., and Lothe, J. L., *Theory of Dislocations*, McGraw Hill, New York, N.Y., 1968.
13. Ingraffea, A. R., and Gerstle, W. H., "Non-Linear Fracture Models for Discrete Crack Propagation," *Applications of Fracture Mechanics to Cementitious Composites*, S. P. Shah, Ed., Martinis Nijhoff, pub., 1985, pp. 247–286.
14. Kobayashi, A. S., Hawkins, N. M., and Barker, D. B., "Fracture Process Zone of Concrete," *Applications of Fracture Mechanics to Cementitious Composites*, S. P. Shah, Ed., Martinis Nijhoff, pub., 1985, pp. 25–50.
15. Lenain, J. C., and Bunsell, A. R., "The Resistance to Crack Growth of Asbestos Cement," *Journal of Materials Science*, 14, 1979, pp. 321–332.
16. Li, V. C., "Fracture Resistance Parameters for Cementitious Materials and Their Experimental Determinations," *Applications of Fracture Mechanics to Cementitious Composites*, S. P. Shah, Ed., Martinis Nijhoff, pub., 1985, pp. 431–449.
17. Liang, E. W., "Nonlinear Models and Analysis of Discrete Cracks in Tension Softening Materials," presented to the Massachusetts Institute of Technology, at Cambridge, Mass., in 1985, in partial fulfillment of the requirements for the degree of Master of Science in Civil Engineering.
18. Majumdar, A. J., and Walton, P. L., "Fracture Processes in Fiber Reinforced Cement Sheets," *Applications of Fracture Mechanics to Cementitious Composites*, S. P. Shah, Ed., Martinis Nijhoff, pub., 1985, pp. 157–186.
19. Palmer, A. C., and Rice, J. R., "The Growth of Slip Surfaces in the Progressive Failure of Overconsolidated Clay Slopes," *Proceedings of the Royal Society of London*, A332, 1973, p. 527.
20. Petersson, P. E., "Fracture Energy of Concrete: Practical Performance and Experimental Results," *Cement and Concrete Research*, Vol. 10, 1980, pp. 91–100.
21. Reinhardt, H. W., "Fracture Mechanics of an Elastic Softening Material like Concrete," HERON, Vol. 29, No. 2, 1984, pp. 5–41.
22. Rice, J. R., "A Path Independent Integral and the Approximate Analysis of Strain Concentrations by Notches and Cracks," *Journal of Applied Mechanics*, ASME, 1968, pp. 379–386.
23. Rice, J. R., "The Mechanics of Earthquake Rupture," *Physics of the Earth's Interior*, Proceedings of the International School of Physics "Enrico Fermi," A. M. Dziewonski, and E. Boschi, Eds., Italian Physical Society, printed by North Holland, Amsterdam, 1980, pp. 555–649.
24. Slate, F. O., "X-Ray Technique for Studying Cracks in Concrete, with Em-

phasis on Methods Developed and used at Cornell Univ.," *Fracture Mechanics of Concrete*, F. H. Whittman, Ed., Elsevier Science Publishers, The Netherlands, 1983, pp. 75–84.
25. Swamy, R. N., "Linear Elastic Fracture Mechanics Parameters of Concrete," *Fracture Mechanics of Concrete*, F. H. Whittman, Ed., Elsevier Science Publishers, The Netherlands, 1983, pp. 411–461.
26. Tada, H., Paris, P. C., and Irwin, G. R., *The Stress Analysis of Cracks Handbook*, Del Research Corp., Hellertown, Pa., 1973.
27. Visalvanich, K., and Naaman, A. W., "Fracture Model of Fiber Reinforced Concrete," *ACI Journal*, Vol. 80, No. 2, 1983, pp. 128–138.
28. Wecharatana, M., and Shah, S. P., "Predictions of Nonlinear Fracture Process Zone in Concrete," *Journal of Engineering Mechanics*, ASCE, Vol. 109, No. 5, 1983, pp. 1400–1413.
29. Wecharatana, M., and Shah, S. P., "A Model for Predicting Fracture Resistance of Fiber Reinforced Concrete," *Cement and Concrete Research*, Vol. 13, 1983, pp. 819–829.

Attenuation of Shocks by Viscoelastic Support

By Marek Elżanowski[1] and Marcelo Epstein,[2] M. ASCE

Abstract: The method of singular surfaces was used in a recent paper to develop a numerical procedure for calculating the growth and decay of the amplitude of shock waves propagating into a one-dimensional nonlinearly elastic body. Here we extend this approach to estimate the influence of such external effects as elastic support and viscous friction on the propagation of shocks. We conclude that even in the case of a homogeneous linearly elastic material these external effects account for some attenuation of the amplitude of the shock and/or the secondary waves. Further analysis of a nonlinear elastic material readily shows that an increase in the viscosity produces, among other things, a slower growth of the shock amplitude and that for some critical value it will even start with a decay. Numerical examples illustrate the applicability of the technique in the case of a homogeneous nonlinear elastic body subjected to external viscous friction.

Introduction

In a recent article (2), we have proposed a numerical procedure for calculating the decay or growth of the amplitude of a strong shock propagating into a one-dimensional nonlinearly elastic medium. The basis for the method is the formulation and subsequent approximate solution of an infinite system of ordinary differential equations governing the speed of propagation of the shock, its amplitude and the amplitudes of the subsidiary weak waves traveling with the shock. In formulating this system use was made of the so-called iterated compatibility conditions provided by the singular surface approach (1), as opposed to attempting the global solution of the hyperbolic system of conservation laws (3) where, except for particularly simple initial conditions, the global solution is not available. On the other hand, it is often the case that only the events taking place at the wave front are of any practical significance and, as shown through numerical examples in Ref. 2, the proposed algorithm readily provides such an information. It should be noted, however, that the extension of the algorithm for two- and three-dimensional problems is extremely difficult.

In the present work, we extend the approach of Ref. 2 to include the influence of external effects of the nature of elastic supports and/or viscous friction as provided, for instance, by the soil surrounding a foundation pile. From the physical point of view these effects will account for some attenuation of the amplitude of the shock and/or the secondary waves even in the case of a homogeneous linearly elastic material, where, in the absence of these extra constraints, the shock and its host of weaker

[1]Research Assoc., Dept. of Mech. Engrg., Univ. of Calgary, Calgary, Alberta, Canada.
[2]Prof., Dept. of Mech. Engrg., Univ. of Calgary, Calgary, Alberta, Canada.
Note.—Discussion open until November 1, 1986. To extend the closing date one month, a written request must be filed with the ASCE Manager of Journals. The manuscript for this paper was submitted for review and possible publication on August 30, 1985. This paper is part of the ***Journal of Engineering Mechanics***, Vol. 112, No. 6, June, 1986. ©ASCE, ISSN 0733-9399/86/0006-0587/$01.00. Paper No. 20667.